

# Learning the dynamics of gluon ladders at intermediate $x$ in inclusive production of $J/\psi$ meson in proton-proton collisions at RHIC energies

S. P. Baranov\*

*P.N. Lebedev Institute of Physics, Lenin avenue 53, Moscow 119991, Russia*

A. Szczurek†

*Institute of Nuclear Physics PAN, PL-31-342 Cracow, Poland and*

*University of Rzeszów, PL-35-959 Rzeszów, Poland*

(Dated: February 6, 2020)

Inclusive cross sections for  $J/\psi$  production in proton-proton collisions were calculated in the  $k_t$ -factorization approach for the RHIC energy. Several mechanisms were considered, including direct color-singlet mechanism, radiative decays of  $\chi_c$  mesons, decays of  $\psi'$ , open-charm associated production of  $J/\psi$  as well as weak decays of B mesons. Different unintegrated gluon distributions from the literature were used. We find that radiative  $\chi_c$  decays and direct color-singlet contributions constitute the dominant mechanism of  $J/\psi$  production. These process cannot be consistently treated within collinear-factorization approach. The results are compared with recent RHIC data. The new precise data at small transverse momenta impose stringent constraints on UGDFs. Some UGDFs are inconsistent with the new data. The Kwieciński UGDFs give the best description of the data. In order to verify the mechanism suggested here we propose  $J/\psi$  – jet correlation measurement and an independent measurement of  $\chi_c$  meson production in  $\pi^+\pi^-$  and/or  $K^+K^-$  decay channels. Finally, we address the issue of  $J/\psi$  spin alignment.

PACS numbers: 12.38Bx, 13.85Ni, 14.40Gx

## I. INTRODUCTION

For the last decade, the inclusive production of  $J/\psi$  mesons was a serious theoretical puzzle challenging our understanding of QCD, parton model, and the bound state formation dynamics. The roots of the puzzling  $J/\psi$  history trace back to the middle 1990s, when the data on  $J/\psi$  and  $\Upsilon$  hadroproduction cross sections [1]–[3] revealed a more than one order-of-magnitude discrepancy with theoretical expectations. This fact has induced extensive theoretical activity and led to the introduction of new production mechanisms, known as the color-octet model [4] and gluon vector dominance model [5]. Since then, the color-octet model has been believed to give the most likely explanation of the quarkonium production phenomena, although there were also some indications that it was not working well. The situation became even more intriguing after the measurements of  $J/\psi$  spin alignment [6]–[7] have been carried out, and the experiment, once again, has demonstrated dramatic disagreement with the newly accepted and commonly trusted theory.

At the same time, it has been shown that the incorporation of the usual color-singlet production scheme with the  $k_t$ -factorization approach can provide a reasonable and consistent picture of the phenomenon under study in its entirety. Within the latter approach, a good description of data on the production of  $J/\psi$ ,  $\chi_c$ , and  $\Upsilon$  mesons both at the Tevatron [8] and HERA [9] has been achieved, and even a solution to the  $J/\psi$  spin alignment problem has been guessed [8, 10]. The issue of the quarkonium production mechanism continues to be under intense debate.

Recently, the PHENIX collaboration at the BNL Relativistic Heavy Ion Collider (RHIC) has measured inclusive  $J/\psi$  production in elementary proton-proton collisions. While for the RHIC community the elementary  $pp$  cross section is only the baseline for the nuclear case, we wish to demonstrate that the elementary data by itself constitute a very valuable information about QCD dynamics in the region of intermediate  $x \simeq 10^{-2}$ – $10^{-1}$ . In our paper we present a detailed analysis of RHIC data based on the  $k_t$ -factorization approach and a large variety of unintegrated gluon distribution functions (UGDFs). We show that the new precise data at small  $J/\psi$  transverse momenta impose stringent constraints on UGDFs and, consequently, stimulate better understanding of the underlying gluon dynamics.

The outline of the paper is the following. In Sec. II we describe the production mechanisms employed in our analysis and discuss the different parametrizations of UGDFs. In Sec. III we compare our theoretical predictions with

---

\*Electronic address: baranov@sci.lebedev.ru

†Electronic address: antoni.szczurek@ifj.edu.pl

experimental results and derive new predictions on the quantities which at yet have not been measured but could serve as important cross-check of our understanding of the reaction mechanism. Our findings and recommendations for the forthcoming experiments are summarized in Sec. IV.

## II. FORMALISM

### A. Different mechanisms of $J/\psi$ production

In this paper, we take into account a number of different mechanisms leading to the appearance of  $J/\psi$  mesons in the final state (of course, they are not thought to be all of equal importance). The considered mechanisms are the following.

Direct color-singlet  $J/\psi$  production via gluon-gluon fusion

$$g + g \rightarrow J/\psi + g; \quad (1)$$

direct production of  $\psi'$  meson

$$g + g \rightarrow \psi' + g \quad (2)$$

and its subsequent decay  $\psi' \rightarrow J/\psi + X$ ;

production of  $P$ -wave charmonium states  $\chi_{cJ}$  ( $J = 0, 1, 2$ )

$$g + g \rightarrow \chi_{cJ} \quad (3)$$

followed by their radiative decays  $\chi_{cJ} \rightarrow J/\psi + \gamma$ ;

production of  $b$  quarks and antiquarks

$$g + g \rightarrow b + \bar{b} \quad (4)$$

followed by their fragmentation into  $B$  mesons and subsequent weak decays  $B \rightarrow J/\psi + X$ ;

production of  $J/\psi$  mesons in association with unbound charmed quarks

$$g + g \rightarrow J/\psi + c + \bar{c}. \quad (5)$$

Examples of the relevant Feynman diagrams for all the mentioned processes are shown in Fig. 1. Every subprocess is accompanied by the emission of gluon jets, as is shown in Fig. 2.

A few words are in order to describe the formation of  $c\bar{c}$  bound states. First of all, it should be noted that the amplitudes of the subprocesses (1)-(3), (5) contain projection operators  $J(S, L)$ , which guarantee the proper quantum numbers of the  $c\bar{c}$  state under consideration. These operators read for the different spin and orbital angular momentum states [11, 12]:

$$J(^1S_0) \equiv J(S=0, L=0) = \gamma_5 (\not{p}_c + m_c)/m_\psi^{1/2}, \quad (6)$$

$$J(^3S_1) \equiv J(S=1, L=0) = \not{\epsilon}(S_z) (\not{p}_c + m_c)/m_\psi^{1/2}, \quad (7)$$

$$J(^3P_J) \equiv J(S=1, L=1) = (\not{p}_{\bar{c}} - m_c) \not{\epsilon}(S_z) (\not{p}_c + m_c)/m_\psi^{3/2}, \quad (8)$$

where  $m_\psi$  is the mass of the  $c\bar{c}$  state and  $m_c = m_\psi/2$  the mass of the charmed quark. States with various projections of the spin momentum onto the  $z$  axis are represented by the polarization vector  $\epsilon(S_z)$ .

The probability for the two quarks to form a meson depends on the bound state wave function  $\Psi(q)$ . In the nonrelativistic approximation which we are using here, the relative momentum  $q$  of the quarks in the bound state is treated as a small quantity. So, it is useful to represent the quark momenta as  $p_c = p_\psi/2 + q$ ,  $p_{\bar{c}} = p_\psi/2 - q$ . Then, we multiply the matrix elements by  $\Psi(q)$  and perform integration with respect to  $q$ . The integration is performed after expanding the integrand around  $q = 0$ :

$$\mathcal{M}(q) = \mathcal{M}|_{q=0} + (\partial\mathcal{M}/\partial q^\alpha)|_{q=0} q^\alpha + \dots \quad (9)$$

Since the expressions for  $\mathcal{M}|_{q=0}$ ,  $(\partial\mathcal{M}/\partial q^\alpha)|_{q=0}$ , etc. are no longer dependent on  $q$ , they may be factored outside the integral sign. A term-by-term integration of this series then yields [12]:

$$\int \frac{d^3q}{(2\pi)^3} \Psi(q) = \frac{1}{\sqrt{4\pi}} \mathcal{R}(x=0), \quad (10)$$

$$\int \frac{d^3q}{(2\pi)^3} q^\alpha \Psi(q) = -i\epsilon^\alpha(L_z) \frac{\sqrt{3}}{\sqrt{4\pi}} \mathcal{R}'(x=0), \quad (11)$$

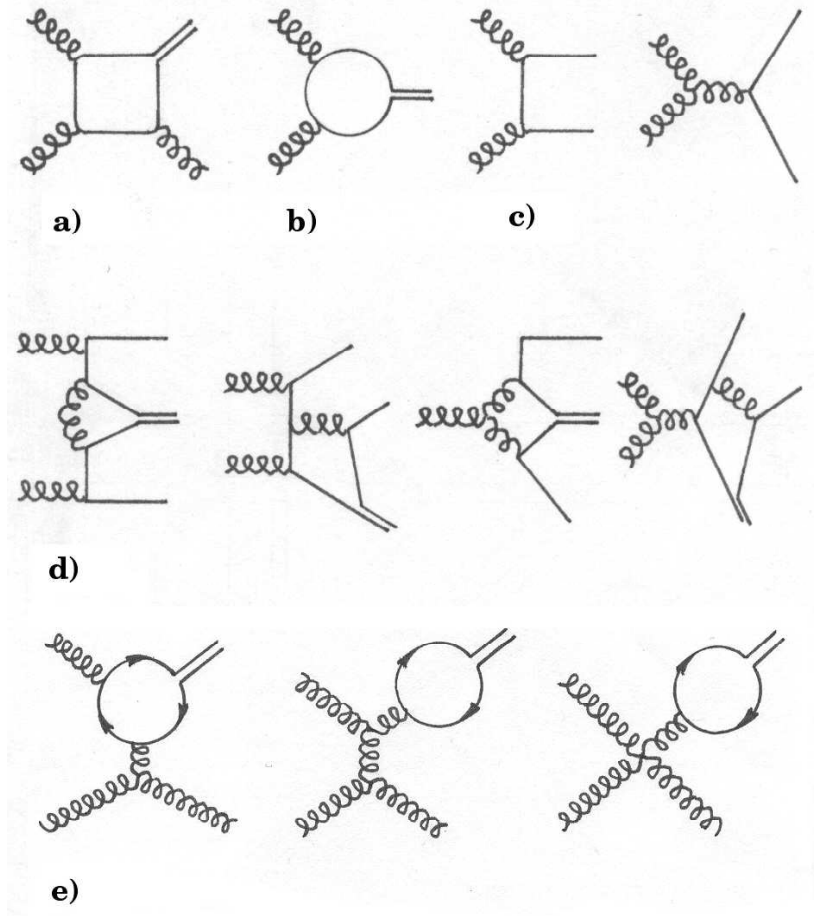


FIG. 1: Processes included in our approach: (a) direct color-singlet production, (b) production of  $\chi_c$  mesons, (c) open bottom quark production, (d) open-charm associated production, (e) color-octet production

etc., where  $\mathcal{R}(x)$  is the wave function in the coordinate representation (the Fourier transform of  $\Psi(q)$ ). The first term contributes only to  $S$ -waves, but vanishes for  $P$ -waves because  $\mathcal{R}_P(0) = 0$ . On the contrary, the second term contributes only to  $P$ -waves, but vanishes for  $S$ -waves because  $\mathcal{R}'_S(0) = 0$ . States with various projections of the orbital angular momentum onto the  $z$  axis are represented by the polarization vector  $\epsilon(L_z)$ . The numerical values of the wave functions are either known from the leptonic decay widths (for  $J/\psi$  and  $\psi'$  mesons) or can be taken from potential models (for  $\chi_{cJ}$  mesons).

When calculating the spin average of the matrix elements squared, we adopt the  $k_t$ -factorization prescription [13] for the off-shell gluon spin density matrix:

$$\overline{\epsilon^\mu \epsilon^{*\nu}} = k_T^\mu k_T^\nu / |k_T|^2, \quad (12)$$

where  $k_T$  is the component of the gluon momentum perpendicular to the beam axis, and the bar stands for the averaging over the gluon spin. In the collinear limit, when  $k_T \rightarrow 0$ , this expression converges to the ordinary  $\overline{\epsilon_g^\mu \epsilon_g^{*\nu}} = -\frac{1}{2} g^{\mu\nu}$ . In all other respects, the evaluation of the diagrams is straightforward and follows the standard QCD Feynman rules. This has been done using the algebraic manipulation systems FORM [14] and REDUCE [15].

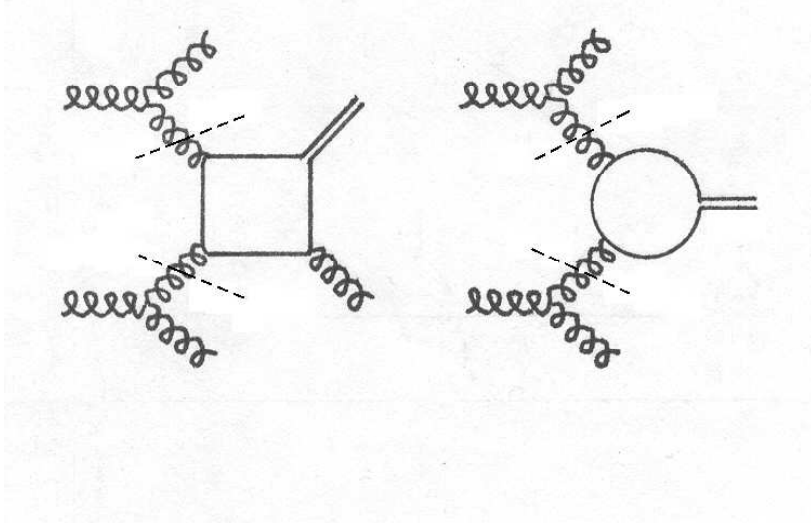


FIG. 2: Application of UGDs to inclusive production of  $J/\psi$  (left) and  $\chi_c$  (right). The upper and the lower parts of these diagrams are included in the  $k_T$  evolution of gluon densities. The emitted gluons can realise in the final state hadronic jets.

For the direct production mechanism (1) the fully differential cross section reads

$$d\sigma(pp \rightarrow \psi X) = \frac{\pi\alpha_s^3 |\mathcal{R}(0)|^2}{\hat{s}^2} \frac{1}{4} \sum_{\text{spins}} \frac{1}{64} \sum_{\text{colors}} |\mathcal{M}(gg \rightarrow \psi g)|^2 \times \mathcal{F}_g(x_1, k_{1T}^2, \mu^2) \mathcal{F}_g(x_2, k_{2T}^2, \mu^2) dk_{1T}^2 dk_{2T}^2 dp_{\psi T}^2 dy_\psi dy_\psi \frac{d\phi_1}{2\pi} \frac{d\phi_2}{2\pi} \frac{d\phi_\psi}{2\pi}, \quad (13)$$

where  $\phi_1$ ,  $\phi_2$  and  $\phi_3$  are the azimuthal angles of the initial and final gluons, and  $y_\psi$  and  $\phi_\psi$  the rapidity and the azimuthal angle of  $J/\psi$  particle. The explicit expressions for the parton level matrix elements  $|\mathcal{M}(gg \rightarrow \psi g)|^2$  are presented in Ref. [8].

The phase space physical boundary is determined by the inequality [16]

$$G(\hat{s}, \hat{t}, k_3^2, k_1^2, k_2^2, m_\psi^2) \leq 0, \quad (14)$$

with  $k_1$ ,  $k_2$  and  $k_3$  being the initial and final gluon momenta,  $\hat{s} = (k_1 + k_2)^2$ ,  $\hat{t} = (k_1 - p_\psi)^2$ , and  $G$  is the standard kinematic function [16]. The initial gluon momentum fractions  $x_1$  and  $x_2$  appearing in the unintegrated gluon distribution functions  $\mathcal{F}_g(x_i, k_{iT}^2, \mu^2)$  are calculated from the energy-momentum conservation laws in the light cone projections:

$$\begin{aligned} (k_1 + k_2)_{E+p_{||}} &= x_1 \sqrt{s} = m_{\psi T} \exp(y_\psi) + |k_{3T}| \exp(y_3), \\ (k_1 + k_2)_{E-p_{||}} &= x_2 \sqrt{s} = m_{\psi T} \exp(-y_\psi) + |k_{3T}| \exp(-y_3), \end{aligned} \quad (15)$$

where  $m_{\psi T} = (m_\psi^2 + |p_{\psi T}|^2)^{1/2}$ .

The production scheme of  $\psi'$  meson (2) is identical to that of  $J/\psi$ , and only the numerical value of the wave function  $|\mathcal{R}(0)|^2$  is different. In both cases, the values of the wave functions were extracted from the known leptonic decay widths [17] using the formula  $|\mathcal{R}(0)|^2 = \Gamma_{ee} m_\psi^2 / (4\alpha^2 e_c^2) [1 - 16\alpha_s / (3\pi)]$  and were set equal to  $|\mathcal{R}_{J/\psi}(0)|^2 = 0.8 \text{ GeV}^3$  for  $J/\psi$  meson, and  $|\mathcal{R}_{\psi'}(0)|^2 = 0.4 \text{ GeV}^3$  for  $\psi'$  meson. To calculate the feed-down to  $J/\psi$  states, the  $\psi'$  production cross section has to be multiplied by the branching fraction  $Br(\psi' \rightarrow J/\psi X) = 56\%$  [17].

For the production of  $\chi_{cJ}$  mesons via the subprocess (3) we have

$$d\sigma(pp \rightarrow \chi_{cJ} X) = \frac{12\pi^2 \alpha_s^2 |\mathcal{R}'(0)|^2}{x_1 x_2 s \lambda^{1/2}(\hat{s}, k_1^2, k_2^2)} \frac{1}{4} \sum_{\text{spins}} \frac{1}{64} \sum_{\text{colors}} |\mathcal{M}'(gg \rightarrow \chi_{cJ})_{q=0}|^2 \times \mathcal{F}_g(x_1, k_{1T}^2, \mu^2) \mathcal{F}_g(x_2, k_{2T}^2, \mu^2) dk_{1T}^2 dk_{2T}^2 dy_\chi \frac{d\phi_1}{2\pi} \frac{d\phi_2}{2\pi}. \quad (16)$$

The explicit expressions for the parton level matrix elements  $|\mathcal{M}(gg \rightarrow \chi_{cJ})|^2$  are presented in Ref. [8]. The numerical value of the wave function is taken from the potential model [18]:  $|\mathcal{R}'_\chi(0)|^2 = 0.075 \text{ GeV}^5$ . The decay branchings

to  $J/\psi$  meson are known to be [17]  $Br(\chi_{cJ} \rightarrow J/\psi\gamma) = 0.013, 0.35,$  and  $0.20$  for  $J = 0, 1,$  and  $2,$  respectively. Here, the off-shell gluon flux factor is defined as  $F = 2\lambda^{1/2}(\hat{s}, k_1^2, k_2^2)$ , according to the general definition given by Eq.(2.3) in Ref. [16]. For all other subprocesses one can use the approximation  $\lambda^{1/2}(\hat{s}, k_1^2, k_2^2) \simeq \hat{s} \simeq x_1 x_2 s$ , but it is not suitable for the present case because the invariant mass of the final state is small and the difference between  $\hat{s} \equiv m_\chi^2$  and  $x_1 x_2 s \equiv m_{\chi,t}^2$  can make pronounced effect on the  $p_T$  spectrum. The numerical accuracy of the above definition was tested in a toy calculation regarding the leptonic production of  $\chi_{cJ}$  mesons via photon-photon fusion:  $e + e \rightarrow e' + e' + \chi_c$ . We have compared the exact  $\mathcal{O}(\alpha^4)$  result with a number of calculations based on Equivalent Photon Approximation and using different definitions of the effective photon flux (such as  $F = 2\hat{s}$ ,  $F = 2x_1 x_2 s$ , etc.). We find that the " $\lambda^{1/2}$ " definition is in the best agreement with exact calculation.

For the production of beauty quarks in (4) we have

$$d\sigma(pp \rightarrow b\bar{b}X) = \frac{4\pi\alpha_s^2}{\hat{s}^2} \frac{1}{4} \sum_{\text{spins}} \frac{1}{64} \sum_{\text{colors}} |\mathcal{M}(gg \rightarrow b\bar{b})|^2 \times \mathcal{F}_g(x_1, k_{1T}^2, \mu^2) \mathcal{F}_g(x_2, k_{2T}^2, \mu^2) dk_{1T}^2 dk_{2T}^2 dp_{bT}^2 dy_b dy_{\bar{b}} \frac{d\phi_1}{2\pi} \frac{d\phi_2}{2\pi} \frac{d\phi_b}{2\pi}. \quad (17)$$

The explicit expressions for the parton level matrix elements  $|\mathcal{M}(gg \rightarrow b\bar{b})|^2$  can be found elsewhere [19]. In calculations the  $b$ -quark mass was set to  $m_b = 4.5$  GeV. Further on, the produced  $b$ -quarks undergo fragmentation into  $B$ -mesons according to the Peterson fragmentation function [20] with  $\epsilon=0.006$ . The outgoing  $B$ -mesons undergo then a decay according to the three body decay mode  $B \rightarrow J/\psi + K + \pi$ , to which the net effective branching fraction [17] was attributed:  $Br(b \rightarrow J/\psi X) = 1.16\%$  (resp.,  $Br(b \rightarrow \psi' X) = 0.48\%$ ). This decay mode was taken as a typical representative for all  $B$ -meson decays. As the decay matrix elements were unknown, the decays were generated according to the phase space. However, the fine details of fragmentation and decay are rather unimportant for our purposes, because  $b$ -quarks play only marginal role at RHIC energies.

Finally, for the charm-associated production (5) we write

$$d\sigma(pp \rightarrow \psi c\bar{c}X) = \frac{\alpha_s^4}{4\hat{s}^2} |\mathcal{R}(0)|^2 \frac{1}{4} \sum_{\text{spins}} \frac{1}{64} \sum_{\text{colors}} |\mathcal{M}(gg \rightarrow \psi c\bar{c})|^2 \times \mathcal{F}_g(x_1, k_{1T}^2, \mu^2) \mathcal{F}_g(x_2, k_{2T}^2, \mu^2) dk_{1T}^2 dk_{2T}^2 dp_{\psi T}^2 dp_{cT}^2 dy_\psi dy_c dy_{\bar{c}} \frac{d\phi_1}{2\pi} \frac{d\phi_2}{2\pi} \frac{d\phi_\psi}{2\pi} \frac{d\phi_c}{2\pi}. \quad (18)$$

The explicit expressions for the parton level matrix elements  $|\mathcal{M}(gg \rightarrow \psi c\bar{c})|^2$  as well as detailed description of the kinematics are presented in Ref. [21].

To conclude the description of the production mechanisms, it is worth saying that we do not consider any kind of color-octet contributions, as we believe that this model has already demonstrated its incapacity. In fact, we know absolutely no data which would clearly manifest the presence of color-octet contributions. On the contrary, the numerical fits of the color-octet matrix elements based on the Tevatron and HERA data are incompatible with each other. Moreover, the dramatic conflict between the model predictions and the data on  $J/\psi$  spin alignment indicate that the production of vector quarkonia has nothing to do with the color-octet mechanism.

## B. Unintegrated gluon distributions

In general, there are no simple relations between unintegrated and integrated parton distributions. Some of UGDFs in the literature are obtained based on familiar collinear distributions, some are obtained by solving evolution equations, some are just modelled or some are even parametrized. A brief review of unintegrated gluon distributions (UGDFs) that will be used also here can be found in Ref.[35]. We shall not repeat all details concerning those UGDFs here.

In some of approaches one imposes the following relation between the standard collinear distributions and UGDFs:

$$g(x, \mu^2) = \int_0^{\mu^2} f_g(x, \mathbf{k}_t^2, \mu^2) \frac{d\mathbf{k}_t^2}{\mathbf{k}_t^2}. \quad (19)$$

Due to its simplicity the Gaussian smearing of initial transverse momenta is a good and popular reference for other approaches. It allows to study phenomenologically the role of transverse momenta in several high-energy processes. We define a simple unintegrated gluon distributions:

$$\mathcal{F}_g^{Gauss}(x, \kappa^2, \mu_F^2) = x g_i^{coll}(x, \mu_F^2) \cdot f_{Gauss}(\kappa^2), \quad (20)$$

where  $g^{coll}(x, \mu_F^2)$  are standard collinear (integrated) gluon distribution and  $f_{Gauss}(\kappa^2)$  is a Gaussian two-dimensional function:

$$f_{Gauss}(\kappa^2) = \frac{1}{2\pi\sigma_0^2} \exp(-\kappa_t^2/2\sigma_0^2) / \pi. \quad (21)$$

The UGDF defined by Eq.(20) and (21) is normalized such that:

$$\int \mathcal{F}_g^{Gauss}(x, \kappa^2, \mu_F^2) d\kappa^2 = x g_i^{coll}(x, \mu_F^2). \quad (22)$$

At small values of  $x$  the unintegrated gluon distribution can be obtained from integrated distribution as [13]:

$$\mathcal{F}(x, k_t^2) = \frac{d(xg(x, \mu^2))}{d\mu^2} \Big|_{\mu^2=k_t^2}. \quad (23)$$

This method cannot be directly used at small transverse momenta (small factorization scales) and must be supplemented by a further prescription. One possible prescription is a freezing of the gluon distribution at  $k_t^2 < \mu_{fr}^2$ , another a shift of the scale:  $\mu^2 \rightarrow \mu^2 + \mu_s^2$ . Of course  $\mu_{fr}^2$  and  $\mu_s^2$  are bigger than the lowest possible scale for standard collinear distributions. This method cannot be also applied at larger  $x$  as here the scaling violation reverses and a negative values are obtained.

At intermediate and large  $x$  a more careful methods must be used. Kwieciński has shown that the evolution equations for unintegrated parton distributions takes a particularly simple form in the variable conjugated to the parton transverse momentum. In the impact-parameter space the Kwieciński equation takes the following simple form [30]

$$\begin{aligned} \frac{\partial \tilde{f}_{NS}(x, b, \mu^2)}{\partial \mu^2} &= \frac{\alpha_s(\mu^2)}{2\pi\mu^2} \int_0^1 dz P_{qq}(z) \left[ \Theta(z-x) J_0((1-z)\mu b) \tilde{f}_{NS}\left(\frac{x}{z}, b, \mu^2\right) \right. \\ &\quad \left. - \tilde{f}_{NS}(x, b, \mu^2) \right], \\ \frac{\partial \tilde{f}_S(x, b, \mu^2)}{\partial \mu^2} &= \frac{\alpha_s(\mu^2)}{2\pi\mu^2} \int_0^1 dz \left\{ \Theta(z-x) J_0((1-z)\mu b) \left[ P_{qq}(z) \tilde{f}_S\left(\frac{x}{z}, b, \mu^2\right) \right. \right. \\ &\quad \left. \left. + P_{qg}(z) \tilde{f}_G\left(\frac{x}{z}, b, \mu^2\right) \right] - [zP_{qq}(z) + zP_{qg}(z)] \tilde{f}_S(x, b, \mu^2) \right\}, \\ \frac{\partial \tilde{f}_G(x, b, \mu^2)}{\partial \mu^2} &= \frac{\alpha_s(\mu^2)}{2\pi\mu^2} \int_0^1 dz \left\{ \Theta(z-x) J_0((1-z)\mu b) \left[ P_{gq}(z) \tilde{f}_S\left(\frac{x}{z}, b, \mu^2\right) \right. \right. \\ &\quad \left. \left. + P_{gg}(z) \tilde{f}_G\left(\frac{x}{z}, b, \mu^2\right) \right] - [zP_{gq}(z) + zP_{gg}(z)] \tilde{f}_G(x, b, \mu^2) \right\}. \end{aligned} \quad (24)$$

We have introduced here the short-hand notation

$$\begin{aligned} \tilde{f}_{NS} &= \tilde{f}_u - \tilde{f}_{\bar{u}}, \quad \tilde{f}_d - \tilde{f}_{\bar{d}}, \\ \tilde{f}_S &= \tilde{f}_u + \tilde{f}_{\bar{u}} + \tilde{f}_d + \tilde{f}_{\bar{d}} + \tilde{f}_s + \tilde{f}_{\bar{s}}. \end{aligned} \quad (25)$$

The unintegrated parton distributions in the impact factor representation are related to the familiar collinear distributions as follows

$$\tilde{f}_k(x, b=0, \mu^2) = \frac{x}{2} p_k(x, \mu^2). \quad (26)$$

On the other hand, the transverse momentum dependent UPDFs are related to the integrated parton distributions as

$$xp_k(x, \mu^2) = \int_0^\infty d\kappa_t^2 f_k(x, \kappa_t^2, \mu^2). \quad (27)$$

The two possible representations are interrelated via Fourier-Bessel transform

$$\begin{aligned} f_k(x, \kappa_t^2, \mu^2) &= \int_0^\infty db b J_0(\kappa_t b) \tilde{f}_k(x, b, \mu^2), \\ \tilde{f}_k(x, b, \mu^2) &= \int_0^\infty d\kappa_t \kappa_t J_0(\kappa_t b) f_k(x, \kappa_t^2, \mu^2). \end{aligned} \quad (28)$$

The index  $k$  above numerates either gluons ( $k=0$ ), quarks ( $k>0$ ) or antiquarks ( $k<0$ ).

While physically  $f_k(x, \kappa_t^2, \mu^2)$  should be positive, there is no obvious reason for such a limitation for  $\tilde{f}_k(x, b, \mu^2)$ .

In the following we use leading-order parton distributions from Ref.[55] as the initial condition for QCD evolution. The set of integro-differential equations in  $b$ -space was solved by the method based on the discretisation made with the help of the Chebyshev polynomials (see [30]). Then the unintegrated parton distributions were put on a grid in  $x$ ,  $b$  and  $\mu^2$  and the grid was used in practical applications for Chebyshev interpolation.

For the calculation of the direct  $J/\psi$  production here the parton distributions in momentum space are more useful. This calculation requires a time-consuming multi-dimensional integration. An explicit calculation of the Kwieciński UPDFs via Fourier transform for needed in the main calculation values of  $(x_1, \kappa_{1,t}^2)$  and  $(x_2, \kappa_{2,t}^2)$  (see next section) is not possible. Therefore auxiliary grids of the momentum-representation UPDFs are prepared before the actual calculation of the cross sections. These grids are then used via a two-dimensional interpolation in the spaces  $(x_1, \kappa_{1,t}^2)$  and  $(x_2, \kappa_{2,t}^2)$  associated with each of the two incoming partons.

The Kwieciński unintegrated parton distributions were used recently in applications to  $c\bar{c}$  photoproduction [34],  $c\bar{c}$  correlations in nucleon-nucleon collisions [35], production of gauge bosons [40], production of Standard Model Higgs boson [39], inclusive production of pions [42], production of direct photons [37]. Good agreement with experimental data was obtained in the case when the data exist.

In the approach of Ref. [52], based on leading-order perturbative solution of BFKL equation, the unintegrated gluon density  $\mathcal{F}_g(x, k_T^2, \mu^2)$  is calculated as a convolution of the ordinary (collinear) gluon density  $G(x, \mu^2)$  with universal weight factors:

$$\mathcal{F}_g(x, k_T^2, \mu^2) = \int_x^1 \mathcal{G}(\eta, k_T^2, \mu^2) \frac{x}{\eta} G\left(\frac{x}{\eta}, \mu^2\right) d\eta, \quad (29)$$

$$\mathcal{G}(\eta, k_T^2, \mu^2) = \frac{\bar{\alpha}_s}{\eta k_T^2} J_0(2\sqrt{\bar{\alpha}_s \ln(1/\eta) \ln(\mu^2/k_T^2)}), \quad k_T^2 < \mu^2, \quad (30)$$

$$\mathcal{G}(\eta, k_T^2, \mu^2) = \frac{\bar{\alpha}_s}{\eta k_T^2} I_0(2\sqrt{\bar{\alpha}_s \ln(1/\eta) \ln(k_T^2/\mu^2)}), \quad k_T^2 > \mu^2, \quad (31)$$

where  $J_0$  and  $I_0$  stand for Bessel functions (of real and imaginary arguments, respectively), and  $\bar{\alpha}_s = \alpha_s/3\pi$ . The LO GRV set [54] was used in our calculations as the input collinear density. Here the value of  $\alpha_s$  and the scale  $\mu^2$  are parameters of the model. The resulting unintegrated gluon distributions depend on them rather strongly. Sometimes for brevity we shall denote the distribution from Ref.[52] by JB.

### III. RESULTS

Now we shall compare contributions of different processes discussed in the previous section. Here a Monte Carlo method based on the VEGAS routine [22] is used to allow an easy comparison of processes with different number of particles in the final state. In Fig. 3 we show contribution of different mechanisms discussed above to the rapidity distributions of  $J/\psi$  meson for the RHIC energy. In this calculation so-called derivative UGDFs, i.e. the ones obtained by differentiating the standard collinear distributions (see the previous section).

In Fig.4 we show corresponding contributions to the transverse momentum distribution of the  $J/\psi$  meson. In this exploratory calculation the cross section is integrated over the full range of rapidity. We obtain a rather surprising result that the sequential production of  $J/\psi$  mesons via radiative decays of  $\chi_c$  mesons is comparable to or even dominates over the direct color-singlet contribution almost in the whole phase space. The reason can be seen in the fact that the production of  $\chi_{cJ}$  states refers to much lower values of the final state invariant mass,  $m_\chi^2 \ll (p_\psi + p_g)^2$ , giving emphasis to the small  $x$  region, where the gluon distributions are growing up. This property becomes even more pronounced as the 'direct' matrix element (1) vanishes when the emitted final gluon is soft. Our conclusion on the relative size of the direct and indirect contributions is compatible with the preliminary estimates obtained by the CDF collaboration [3].

It is worth noting that the production of  $\chi_c$  mesons can hardly be described in a consistent way within the collinear factorization scheme. The leading order contribution coming from the subprocess (3) shows unphysical  $\delta$ -like  $p_T$  spectrum. The usual lame excuses that the particles produced at zero  $p_T$  disappear in the beam pipe and remain invisible do not work, because the decay products do have nonzero  $p_T$  and, undoubtedly, can be detected. At the same time, introducing the next-to-leading contributions (i.e., the processes with extra gluons in the final state) causes the problem of infrared divergences, which need artificial tricks to regularize them.

It is well known that a large fraction of the  $\psi'$  mesons decays into channels with  $J/\psi$  (BR = 0.56 [17]). This contribution was not considered in the literature and requires a separate discussion. The inclusive cross section for  $\psi'$  can be calculated in exactly the same way (color-singlet model) as the cross section for direct  $J/\psi$  meson production. The decays of  $\psi' \rightarrow J/\psi + X$  change the kinematics only slightly. Finally the  $\psi'$  contribution constitutes about a quarter of the direct (color-singlet) production.

Also the B-meson decay mechanism gives a sizeable contribution at large transverse momenta.

Summarizing, at the RHIC energy the dominant production mechanisms are radiative decays of  $\chi_c(2^+)$  and direct color-singlet mechanism. In the following we shall concentrate exclusively on these two dominant mechanisms.

Let us start with color-singlet mechanism. In Fig.5 we present distributions in rapidity of  $J/\psi$  produced by direct color-singlet mechanism for different UGDFs. The distribution obtained with Ivanov-Nikolaev (IN) glue exceeds the experimental PHENIX data [23], while the other theoretical distributions are smaller than experimental data. This is rather natural as contributions of other mechanisms are not included. The corresponding distributions in transverse momentum are shown in Fig.6 for two different intervals in rapidity. Very similar distributions are obtained for mid- and intermediate rapidity intervals. The result with Ivanov-Nikolaev UGDF exceeds the experimental data in the region of small transverse momenta. This is probably due to an extra nonperturbative contribution at small gluon transverse momenta [31].

Now we shall show results obtained with different UGDFs for radiative decays of  $\chi_c(2^+)$ . The rapidity distribution of corresponding  $J/\psi$  is shown in Fig.7. Different UGDFs give a similar result. The distributions obtained with Ivanov-Nikolaev is slightly higher than those obtained with other distributions. In Fig.8 we show distributions of radiatively produced  $J/\psi$ . The differences in the results for different UGDFs are up to a factor 2 or even larger. Again IN UGDF gives the highest cross section for small transverse momenta.

Finally we would like to show how the sum of the two dominant contributions (direct color-singlet and radiative  $\chi_c(2^+)$  decay) compares with the experimental data from RHIC. The distribution in rapidity is shown in Fig.9 and distributions in transverse momentum in Fig.10. The theoretical cross sections obtained with the Kwieciński, BFKL and Kharzeev-Levin UGDFs stay slightly below the experimental data. This seems to be consistent with the fact that the smaller contributions discussed in Fig.3 and Fig.4 are not included here. They are expected to produce contributions of the order of 30 %.

At the RHIC energy  $W = 200$  GeV the longitudinal momentum fractions of the order  $x \sim 10^{-2} - 10^{-1}$  come into game. This is the place where application of many UGDFs may be questionable. Let us concentrate now on Kwieciński parton distributions, which are constructed for the region of  $x$  under discussion. In the left panel of Fig.11 we show invariant cross section for the direct component as a function of  $J/\psi$  transverse momentum  $p_t$  for mid rapidity range  $-0.35 < y < 0.35$ . We show results for different factorization scales:  $\mu^2 = 10 \text{ GeV}^2$  (dashed) and  $\mu^2 = 100 \text{ GeV}^2$  (dotted) as well as for running scale  $\mu^2 = (m_{1t}^2 + m_{2t}^2)/2$  (solid). In the right panel of Fig.11 we show similar result for  $J/\psi$  coming from the decays of the  $\chi_c(2^+)$ . Here the result depend more strongly on the choice of the scale. The solid line here corresponds to running factorization scale:  $\mu^2 = m_t^2 = m_{\chi_c(2^+)}^2 + p_t^2$ .

In Fig.12 we compare the sum of both processes calculated with running factorization scale with the PHENIX experimental data. A rather good description of the data is obtained. The calculation underestimates the data at small transverse momenta. This is most probably due to the omission of other components, especially the  $\psi'$ -decay component.

Let us concentrate now on correlations between produced  $J/\psi$  and associated gluon(s). In Fig.13 we present two-dimensional distribution in transverse momentum of  $J/\psi$  ( $p_{1t}$ ) and transverse momentum of the associated (the gluon related with the matrix element) gluon ( $p_{2t}$ ) for two different scales of the Kwieciński UGDF. The bigger the scale the bigger the spread of the cross section in the  $(p_{1t}, p_{2t})$  space. This can be understood by the fact that the bigger scales means more gluonic emissions which statistically means the bigger spread. This figure is rather of academic value as in practice there are also gluons emitted in the process of the ladder-type emissions. Strictly speaking, the latter have to be described using a full gluon evolution generator. On the other hand, the relevant effects can also be estimated in an approximate way, as follows. On the average, the gluon transverse momentum increases from the proton line towards the hard interaction block (although there is no strict ordering in the transverse momentum in BFKL equation). So, it is most likely, that the last gluon in the parton ladder has the largest  $k_t$  value. As a rough approximation, one can neglect the transverse momenta of all the other emitted gluons (note that the evolution is in the  $\log(k_t)$  space rather than  $k_t$  space) and use the conservation law in the last splitting vertex to set the  $k'_t$  of the emitted gluon equal to the  $k_t$  of the gluon entering the partonic matrix element:  $k'_t \simeq -k_t$ . The latter is known from the unintegrated gluon distribution. This trick gives an estimate for the transverse momentum of the final state gluon jet.

In Fig.14 we show distributions of the cross section on the plane  $p_t(J/\psi) \times p_t$  (matrix element gluon or last gluon in the ladder) for the Kwieciński UGDF with running scale (left part) and BFKL UGDF (right part). Comparing these distributions we conclude that the gluons from the ladder (LFL - last from the ladder) contribute to lower transverse momenta than those associated with the matrix element  $g + g \rightarrow J/\psi + g$  (ME) for the Kwieciński UGDF, where at

$p_t(\text{gluon}) > 5 \text{ GeV}$  the matrix element gluons dominate over the ladder gluons. For the BFKL gluons the situation is much more complicated as here the distribution for ME gluons and LFL gluons are similar.

In Fig.15 we show average value of transverse momentum of the matrix element gluon (dashed line) and of the last gluon from the ladder (solid line) as a function of  $J/\psi$  transverse momentum. These average values have completely different dependence on  $p_t(J/\psi)$ . While average value of the LFL gluon transverse momentum is only weakly dependent on  $p_t(J/\psi)$ , the average value of the ME gluon transverse momentum grows monotonically with  $p_t(J/\psi)$ . At low  $J/\psi$  transverse momenta  $\langle p_t(\text{LFL}) \rangle \sim \langle p_t(\text{ME}) \rangle$ . At higher  $J/\psi$  transverse momenta  $\langle p_t(\text{LFL}) \rangle < \langle p_t(\text{ME}) \rangle$ . For the Kwieciński distribution this happens at smaller transverse momentum than for the BFKL UGDF.

Up to now we discussed only mechanisms when  $J/\psi$  is produced as one of many hadrons (both mesons and baryons) in the final state. Recently an exclusive process with well defined final state was discussed in the literature (see e.g. [56] and references therein). Due to its specificity this final channel is not included in and process discussed up to now. We wish to discuss now separately a contribution of  $J/\psi$  from the exclusive production  $pp \rightarrow ppJ/\psi$  due to photon-pomeron or pomeron-photon fusion (for details see the analysis in [56]). In Fig.16 we present invariant distribution of  $J/\psi$  calculated as in Ref.[56] for central and intermediate rapidity range. This contribution constitutes only a small fraction of the inclusive cross section and is concentrated mainly at small transverse momenta. The identification of such a component would require a measurement of forward/backward protons in addition to more centrally produced  $J/\psi$ . It is not clear to us if this will be possible with the future RHIC instrumentation. Such a process is currently being analysed at Tevatron [57].

Our calculations presented up to now show that the production of  $J/\psi$  through radiative decays of  $\chi_c$  mesons is one of two dominant mechanisms. It would be worth to verify this theoretical prediction experimentally. This would require measuring the  $\chi_c$  mesons independently. In Fig.17 we show the distributions in rapidity for  $\chi_c(0^+)$ ,  $\chi_c(1^+)$  and  $\chi_c(2^+)$ . These results were obtained with the help of the Kwieciński UGDF, which seems to be the most reliable for the RHIC energy range.

For completeness in Fig.18 we show the corresponding distributions in transverse momentum. In this calculation  $-1 < y < 1$ . We wish to point out that the cross sections show no singularity at small transverse momentum. This contrasts with the collinear factorization predictions, which are either unphysical ( $\delta$ -like) or divergent (if based on a  $2 \rightarrow 2$  subprocess  $g + g \rightarrow \chi_c + g$ ). There is also a significant difference in shape between the transverse momentum distribution for  $\chi_c(1^+)$  meson and those for  $\chi_c(0^+)$  and  $\chi_c(2^+)$  mesons. This property emerges from Landau-Yang theorem which prohibits the coupling of vector states to massless photons (just because of quantum numbers incompatible with Bose statistics). The production of  $\chi_c(1^+)$  states at small  $p_T$  is strongly suppressed because the initial gluons are almost on shell. The suppression goes away at higher  $p_T$ , as the off-shellness of the initial gluons becomes larger. These features are discussed in detail in Ref. [25].

In contrast to transverse momentum distribution of  $J/\psi$  from the color-octet mechanism, the distributions of  $\chi_c$  mesons (and consequently the distribution of  $J/\psi$  from radiative decays) strongly depend on the model of UGDF. In particular, in the limiting case of vanishing initial gluon transverse momenta:  $d\sigma/d^2p_t \propto \delta^2(\vec{p}_t)$ . For illustrating the effect quantitatively in Fig.19 we present transverse momentum distributions of  $\chi_c(2^+)$  for the Gaussian UGDF with different values of the smearing parameter  $\sigma_0 = 0.5, 1, 2 \text{ GeV}$ . The example clearly demonstrates that a measurement of transverse momentum distribution of  $\chi_c$  mesons would open a new and unique possibility to test model unintegrated gluon distributions.

In principle the  $\chi_c$  mesons (mainly  $\chi_c(1^+)$  and  $\chi_c(2^+)$ ) can be identified via photon- $J/\psi$  decay channel. At RHIC the  $\chi_c$  production mechanism could be also identified using the  $\pi^+\pi^-$  and  $K^+K^-$  final channels. The corresponding branching ratios are [17]:

$$\begin{aligned} BR(\chi_c(0^+) \rightarrow \pi^+\pi^-) &= 7.2 \pm 0.6 \times 10^{-3}, \quad BR(\chi_c(0^+) \rightarrow K^+K^-) = 5.4 \pm 0.6 \times 10^{-3}, \\ BR(\chi_c(2^+) \rightarrow \pi^+\pi^-) &= 2.14 \pm 0.25 \times 10^{-3}, \quad BR(\chi_c(2^+) \rightarrow K^+K^-) = 7.7 \pm 1.4 \times 10^{-4}. \end{aligned}$$

Now we are coming to the issue of  $J/\psi$  spin alignment, which was, and still is under intense debates in the literature. We want to stress once again that measuring the polarization of quarkonium states produced at high energies may serve as a crucial test discriminating the different concepts of parton dynamics.

The polarization state of a vector meson is characterized by the spin alignment parameter  $\alpha$  which is defined as a function of any kinematic variable as

$$\alpha(\mathcal{P}) = (d\sigma/d\mathcal{P} - 3d\sigma_L/d\mathcal{P})/(d\sigma/d\mathcal{P} + d\sigma_L/d\mathcal{P}), \quad (32)$$

where  $\sigma$  is the reaction cross section,  $\mathcal{P}$  is a selected kinematical variable and  $\sigma_L$  is the part of cross section corresponding to mesons with longitudinal polarization (zero helicity state). The limiting values  $\alpha = 1$  and  $\alpha = -1$  refer to the totally transverse and totally longitudinal polarizations. Here we consider only the behavior of  $\alpha$  as a function of the  $J/\psi$  transverse momentum:  $\mathcal{P} \equiv |\mathbf{p}_T|$ . The experimental definition of  $\alpha$  is based on measuring the angular distributions of the decay leptons

$$d\Gamma(J/\psi \rightarrow \mu^+\mu^-)/d\cos\theta \sim 1 + \alpha \cos^2\theta, \quad (33)$$

where  $\theta$  is the polar angle of the final state muon measured in the decaying meson rest frame.

The results of our calculations for the kinematic conditions of RHIC are displayed in Fig. 20. In order to show the theoretical uncertainty band connected with the choice of UGDF, we use two different parametrizations, which are known to show the largest difference with each other, namely, the ones proposed in Refs. [13] (called 'derivative' for brevity) and the one from Ref.[52].

The upper panel in Fig. 20 shows the behavior of the spin alignment parameter  $\alpha$  for  $J/\psi$  mesons produced in the direct subprocess (1). The increase in the fraction of longitudinally polarised mesons comes from the increasing virtuality (and longitudinal polarization) of the initial gluons. These predictions shown here are also valid for  $\psi'$  mesons.

As far as the contribution from  $P$ -waves is concerned, nothing is known on the polarisation properties of their decays. If we assume that the quark spin is conserved in radiative transitions, and the emission of a photon only changes the quark orbital momentum (as it is known to be true in the electric dipole transitions in atomic physics,  $\Delta S = 0$ ,  $\Delta L = \pm 1$ ), then the predictions on  $\alpha$  appear to be similar to those made for the direct channel (see lower panel in Fig. 20, dotted curves). If, on the contrary, we assume that the transition  $\chi_c \rightarrow J/\psi + \gamma$  leads to a complete depolarization, then we arrive at a more moderate behavior of the parameter  $\alpha$  (dash-dotted curves in Fig.20). The overall polarization remains slightly longitudinal ( $\alpha \simeq -0.1$ ) in the whole range of  $p_T$  due to the 'direct' contribution. A comparison between the data on  $J/\psi$  and  $\psi'$  polarization at the Tevatron [7] seems to give support to the depolarization hypothesis. The difference between the  $J/\psi$  and  $\psi'$  polarization data can be naturally explained by the presence of the depolarizing contribution in the case of  $J/\psi$  and the absence of this contribution in the case of  $\psi'$ .

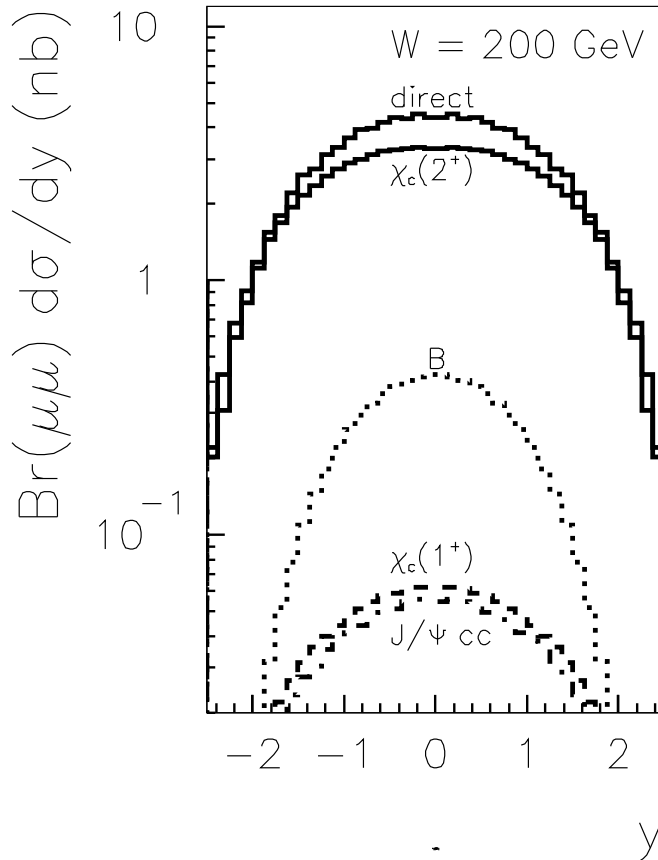


FIG. 3: Contributions of different mechanisms for the production of  $J/\psi$  in  $d\sigma/dy$  distributions. In this calculation we have used simple “derivative UGDF”.

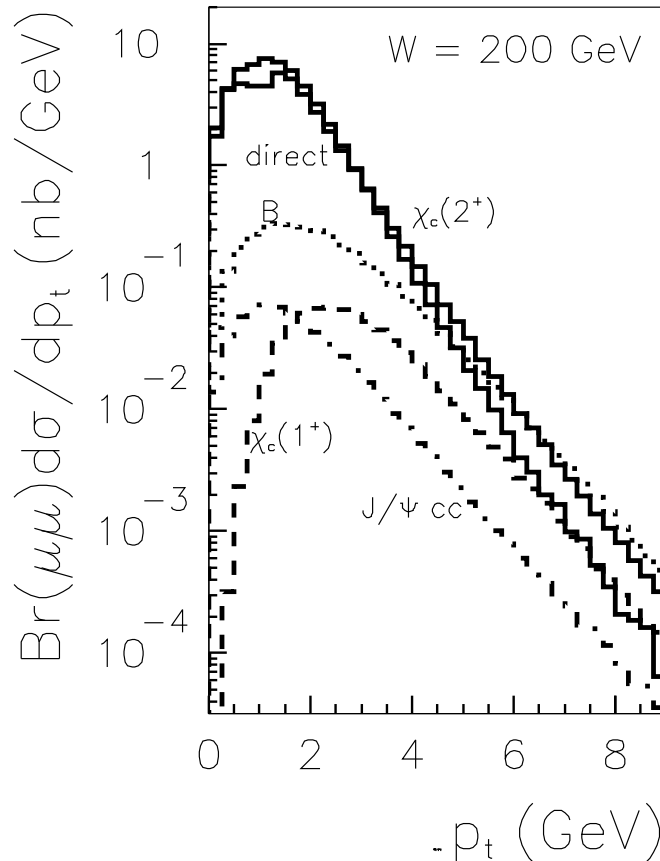


FIG. 4: Contributions of different mechanisms for the production of  $J/\psi$  in  $d\sigma/dp_t$  distributions. In this calculation we have used simple “derivative UGDF”. The cross section is integrated over the full range of rapidity.

#### IV. DISCUSSION AND CONCLUSIONS

We have considered different mechanisms contributing to the inclusive production of  $J/\psi$  mesons in  $pp$  collisions at RHIC kinematics. The outcome of our study is the following.

We have inspected the hierarchy of contributions and found that the dominant piece of the cross section comes from radiative decay of  $\chi_c$  mesons, mainly from  $\chi_c(2^{++})$  state. The second most important mechanism is the direct color-singlet production. The sequential process through the intermediate  $\psi'$  turned out to be nonnegligible and constitutes about a quarter of the direct color-singlet contribution. To our knowledge, these processes were not included in previous calculations in the literature on the subject.

As a by-product, we have demonstrated the advantage of the  $k_t$ -factorization approach in calculating the  $\chi_c$  spectra: the latter can hardly be calculated in a consistent way in the collinear scheme. In order to verify the production mechanism suggested in our analysis, we have proposed an independent measurement of inclusive  $\chi_c$  cross sections in the  $\pi^+\pi^-$  and  $K^+K^-$  decay channels.

We have applied our approach to describe the data on inclusive  $J/\psi$  production recently collected by the PHENIX Collaboration at the BNL. Both rapidity and transverse momentum distributions have been discussed. The new precise data at small  $J/\psi$  transverse momenta appeared to show very strong analysing power, imposing stringent constraints on unintegrated gluon distributions. The best description of the data is obtained with the UGDF proposed by Kwieciński.

Another piece of important information on the underlying gluon dynamics can be extracted from studying kinematic correlations between  $J/\psi$  mesons and coproduced gluon jets. In this paper we have presented our predictions for the

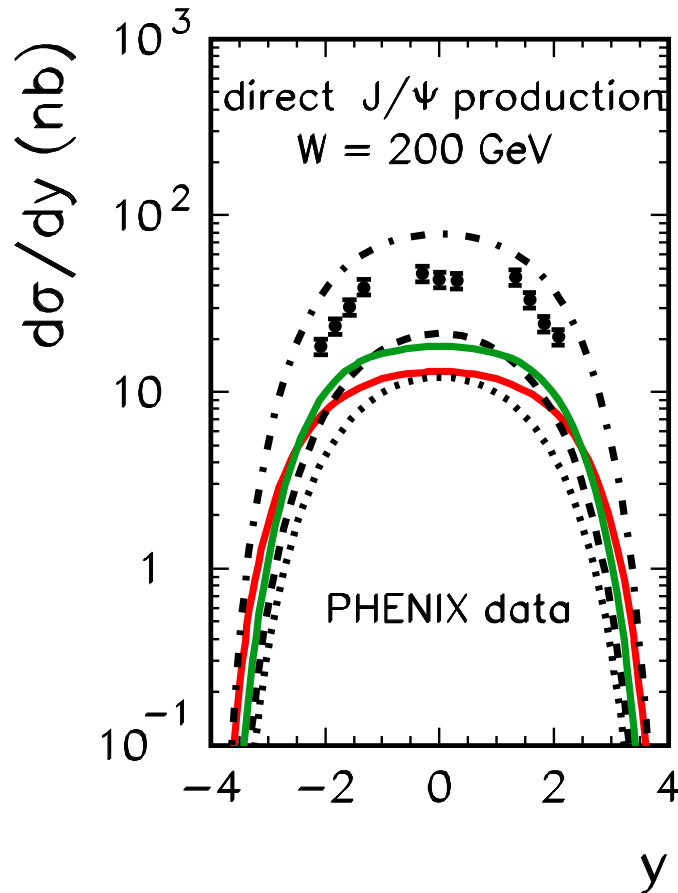


FIG. 5: Direct color-singlet contribution to rapidity distribution of  $J/\psi$  for different models of UGDFs. The solid (red on line) curve corresponds to the Kwieciński UGDF, the dashed line to the Kharzeev-Levin UGDF, the dotted line to the BFKL UGDF, the dash-dotted line to the Ivanov-Nikolaev UGDF. The new PHENIX data are shown as full circles.

two dominant contributing mechanisms.

We have found that discussed recently in the literature exclusive production of  $J/\psi$  due to pomeron-photon or photon-pomeron fusion constitutes only small fraction of the inclusive cross section.

We do not find much room for color-octet contribution which was advocated for some time as a solution to the  $J/\psi$  puzzle.

Finally, we have presented our predictions on  $J/\psi$  spin alignment. The latter can serve as important test discriminating two different concepts of parton model.

In the present paper we have discussed mechanisms of  $J/\psi$  production in elementary collisions. We believe that our findings here may be also useful for nuclear collisions, where  $J/\psi$  suppression was originally suggested as a useful indication of the presence of the quark-gluon plasma.

**Acknowledgments** We are indebted to Abigail Bickley from the PHENIX collaboration for providing us recent experimental data on inclusive  $J/\psi$  production measured at RHIC. Thanks go to Jerzy Bartke for pointing to us the possibility that the  $\psi'$ -decay contribution may be sizeable. This work was partially supported by the grant of the Polish Ministry of Scientific Research and Information Technology number 1 P03B 028 28.

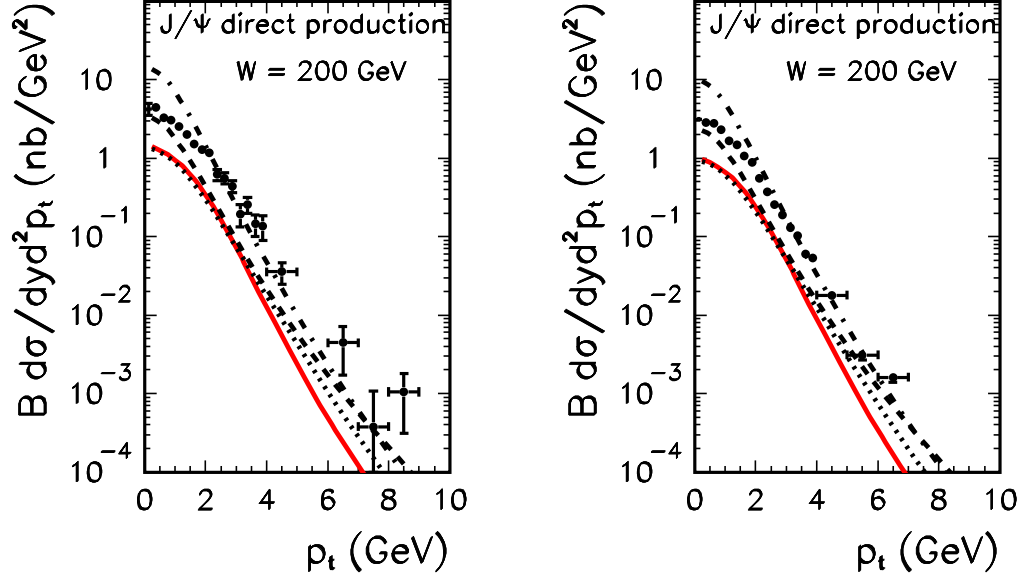


FIG. 6: Direct color-singlet contribution to transverse momentum distribution of  $J/\psi$  for different models of UGDFs for different intervals in rapidity: (a)  $-0.35 < y < 0.35$  (left panel), (b)  $1.2 < |y| < 2.2$  (right panel). The meaning of the curves is the same as in Fig. 5. The new PHENIX data are shown as full circles.

- 
- [1] CDF Collaboration, F. Abe *et al.*, Phys. Rev. Lett. **69**, 3704 (1992); **71**, 2537 (1993); **75**, 1451 (1995); **79**, 578 (1997).
  - [2] CDF Collaboration, F. Abe *et al.*, Phys. Rev. Lett. **86**, 3963 (2001).
  - [3] CDF Collaboration, T. Affolder *et al.*, Phys. Rev. Lett. **84**, 2094 (2000).
  - [4] P. Cho and A. K. Leibovich, Phys. Rev. D **53**, 150 (1996); **53**, 6203 (1996).
  - [5] S. P. Baranov, Phys. Lett. B **388**, 366 (1996).
  - [6] E537 Collaboration, C. Akerlof *et al.*, Phys. Rev. D **48**, 5067 (1993).
  - [7] CDF Collaboration, T. Affolder *et al.*, Phys. Rev. Lett. **85**, 2886 (2000).
  - [8] S. P. Baranov, Phys. Rev. D **66**, 114003 (2002).
  - [9] S. P. Baranov and N. P. Zotov, J. Phys. G **29**, 1395 (2003); A. V. Lipatov and N. P. Zotov, Eur. Phys. J. C **27**, 87 (2003).
  - [10] S. P. Baranov, Phys. Lett. B **428**, 377 (1998).
  - [11] C.-H. Chang, Nucl. Phys. **B172**, 425 (1980); R. Baier and R. Rückl, Phys. Lett. B **102**, 364 (1981); E. L. Berger and D. Jones, Phys. Rev. D **23**, 1521 (1981).
  - [12] H. Krasemann, Z. Phys. C **1**, 189 (1979); G. Guberina, J. Kühn, R. Peccei, and R. Rückl, Nucl. Phys. **B174**, 317 (1980).
  - [13] L. V. Gribov, E. M. Levin, and M. G. Ryskin, Phys. Rep. **100**, 1 (1983); E. M. Levin and M. G. Ryskin, Phys. Rep. **189**, 267 (1990).
  - [14] J. A. M. Vermaseren, Symbolic Manipulations with FORM, published by CAN (Computer Algebra Nederland), Kruislaan 413, 1098, SJ Amsterdam 1991, ISBN 90-74116-01-9.
  - [15] A. C. Hearn, Preprint Utah University CP78 Rev. 4/84 (Rand Publ., Utah, 1984).
  - [16] E. Bycling and K. Kajantie, Particle Kinematics, John Wiley and Sons (Eds.), 1973.
  - [17] Particle Data Group, W.-M. Yao *et al.*, J. Phys. G **33**, 1 (2006).
  - [18] E. J. Eichten and C. Quigg, Phys. Rev. D **52**, 1726 (1995).
  - [19] S. P. Baranov, M. Smižanská, Phys. Rev. D **62**, 014012 (2000).
  - [20] C. Peterson, D. Schlatter, I. Schmitt, and P. Zerwas, Phys. Rev. D **27**, 105 (1983).
  - [21] S. P. Baranov, Phys. Rev. D **73**, 074021 (2006).
  - [22] G.P. Lepage, J. Comput. Phys. **27** 192 (1978).
  - [23] A. Adare *et al.* (PHENIX collaboration), hep-ex/0611020;  
A. Bickley *et al.* (PHENIX collaboration), hep-ph/0701037.
  - [24] F. Yuan and K.-T. Chao, Phys. Rev. **D63** (2001) 034006.
  - [25] S. P. Baranov, Phys. Lett. B **594**, 277 (2004)

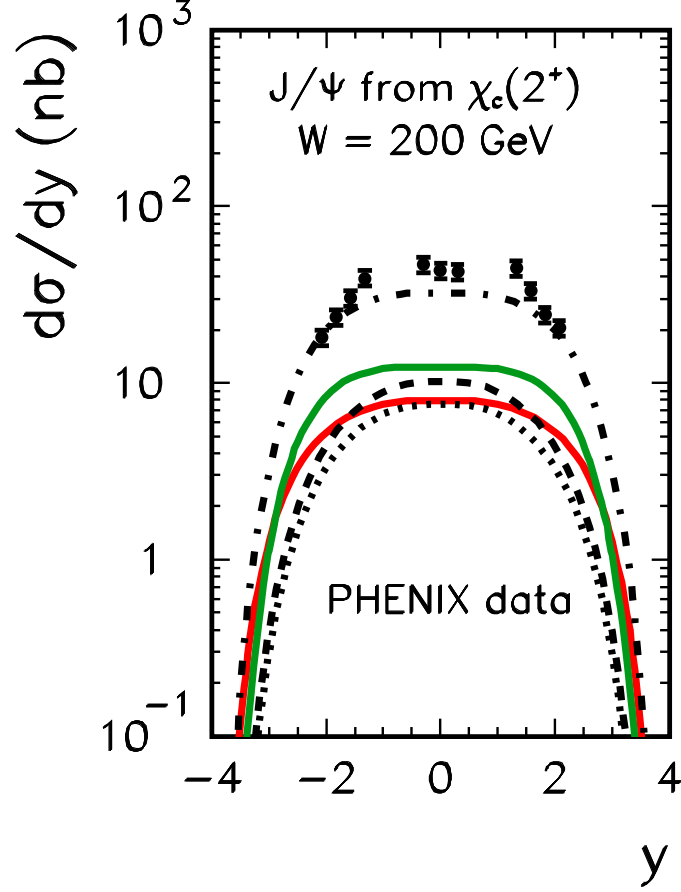


FIG. 7:  $\chi_c$ -decay contribution to rapidity distribution of  $J/\psi$  for different models of UGDFs. The meaning of the curves is the same as in Fig. 5. The new PHENIX data are shown as full circles.

- [26] Ph. Hägler, R. Kirschner, A. Schäfer, L. Szymanowski and O.V. Teryaev, Phys. Rev. Lett. **86** (2001) 1446;  
Ph. Hägler, R. Kirschner, A. Schäfer, L. Szymanowski and O.V. Teryaev, Phys. Rev. **D63** (2001) 077501.
- [27] S.P. Baranov, Phys. Rev. **D66** (2002) 114003.
- [28] S.P. Baranov, Phys. Rev. **D73** (2006) 074021.
- [29] S. Catani, M. Ciafaloni and F. Hautmann, Nucl. Phys. **366** (1991) 135;  
J.C. Collins and R.K. Ellis, Nucl. Phys. **B360** (1991) 3.
- [30] J. Kwieciński, Acta Phys. Polon. **B33** (2002) 1809;  
A. Gawron and J. Kwieciński, Acta Phys. Polon. **B34** (2003) 133;  
A. Gawron, J. Kwieciński and W. Broniowski, Phys. Rev. **D68** (2003) 054001.
- [31] I.P. Ivanov and N.N. Nikolaev, Phys. Rev. **D65** (2002) 054004.
- [32] S.P. Baranov and M. Smizanska, Phys. Rev. **D62** (2000) 014012.
- [33] A.V. Lipatov, V.A. Saleev and N.P. Zotov, hep-ph/0112114;  
S.P. Baranov, A.V. Lipatov and N.P. Zotov, hep-ph/0302171, Yad. Fiz. **67** (2004) 856.
- [34] M. Łuszczak and A. Szczurek, Phys. Lett. **B594** (2004) 291.
- [35] M. Łuszczak and A. Szczurek, Phys. Rev. **D73** (2006) 054028.
- [36] A.V. Lipatov and N.P. Zotov, Phys. Rev. **D72** (2005) 054002.
- [37] T. Pietrycki and A. Szczurek, hep-ph/0606304, Phys. Rev. **D75** (2007) 014023.
- [38] A.V. Lipatov and N.P. Zotov, Eur. Phys. J. **C44** (2005) 559.
- [39] M. Łuszczak and A. Szczurek, Eur. Phys. J. **C46** 123 (2006).
- [40] J. Kwieciński and A. Szczurek, Nucl. Phys. **B680** (2004) 164.
- [41] A. Szczurek, Acta Phys. Polon. **B34** (2003) 3191.
- [42] M. Czech and A. Szczurek, Phys. Rev. **C72** (2005) 015202;

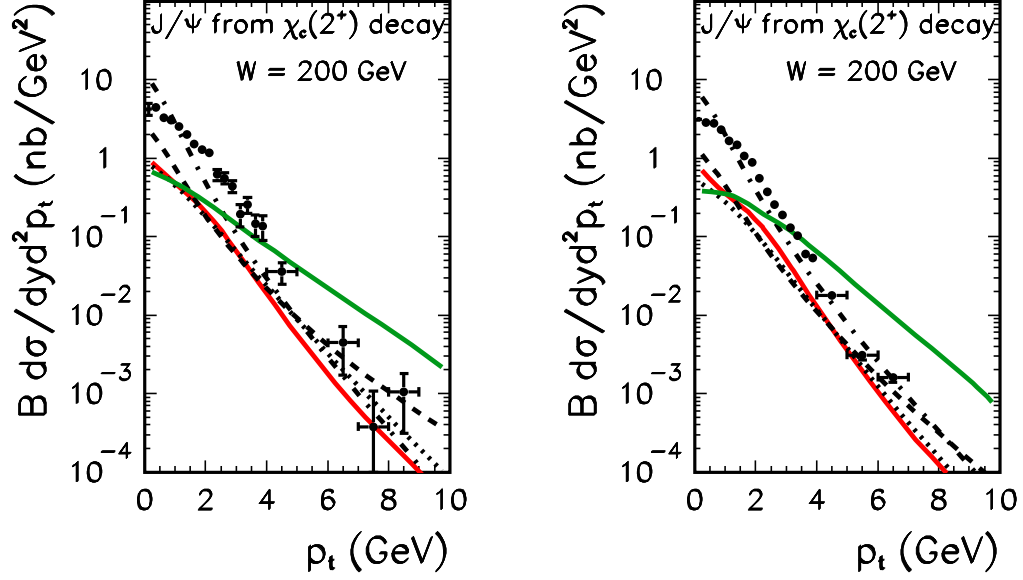


FIG. 8:  $\chi_c$ -decay contribution to transverse momentum distribution of  $J/\psi$  for different models of UGDFs for different intervals in rapidity: (a)  $-0.35 < y < 0.35$  (left panel), (b)  $1.2 < |y| < 2.2$  (right panel). The meaning of the curves is the same as in Fig. 5. The new PHENIX data are shown as full circles.

- M. Czech and A. Szczurek, J. Phys. **G32** (2006) 1253.
- [43] A. Szczurek, N.N. Nikolaev, W. Schäfer and J. Speth, Phys. Lett. **B500** (2001) 254.
  - [44] U. D'Alesio and F. Murgia, Phys. Rev. **D70** (2004) 074009.
  - [45] V.D. Barger and R.J.N. Phillips, "Collider physics", Addison-Wesley Publishing Company, 1987
  - [46] M.A. Kimber, A.D. Martin and M.G. Ryskin, Eur. Phys. J. **C12** (2000) 655;  
M.A. Kimber, A.D. Martin and M.G. Ryskin, Phys. Rev. **D63** (2001) 114027.
  - [47] J. Kwieciński, A.D. Martin and A.M. Staśto, Phys. Rev. **D56** (1997) 3991.
  - [48] E.A. Kuraev, L.N. Lipatov and V.S. Fadin, Sov. Phys. JETP **45** (1977) 199;  
Ya.Ya. Balitskij and L.N. Lipatov, Sov. J. Nucl. Phys. **28** (1978) 822.
  - [49] A.J. Askew, J. Kwieciński, A.D. Martin and P.J. Sutton, Phys. Rev. **D49** (1994) 4402.
  - [50] K.J. Eskola, A.V. Leonidov and P.V. Ruuskanen, Nucl. Phys. **B481** (1996) 704.
  - [51] K. Golec-Biernat and M. Wüsthoff, Phys. Rev. **D60** (1999) 114023-1.
  - [52] J. Blümlein, DESY preprint DESY 95-121 (1995).
  - [53] D. Kharzeev and E. Levin, Phys. Lett. **B523** (2001) 79.
  - [54] M. Glück, E. Reya and A. Vogt, Z. Phys. **C67** (1995) 433.
  - [55] M. Glück, E. Reya and A. Vogt, Eur. Phys. J. **C5** (1998) 461.
  - [56] W. Schäfer and A. Szczurek, arXiv:0705.2887, in print in Phys. Rev. **D**.
  - [57] J. Pinfold, a talk at the international conference PHOTON2007, July 9-13 2007, Paris, France, unpublished.

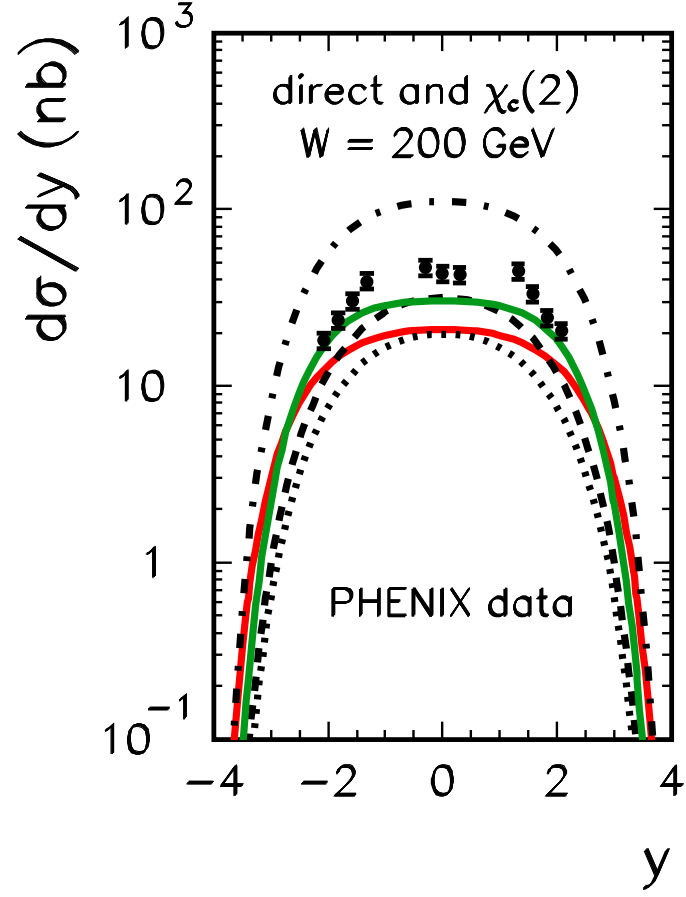


FIG. 9: Direct color-singlet and  $\chi_c(2^+)$  contributions to rapidity distribution of  $J/\psi$  for different models of UGDFs. The meaning of the curves is the same as in Fig. 5. The new PHENIX data are shown as full circles.

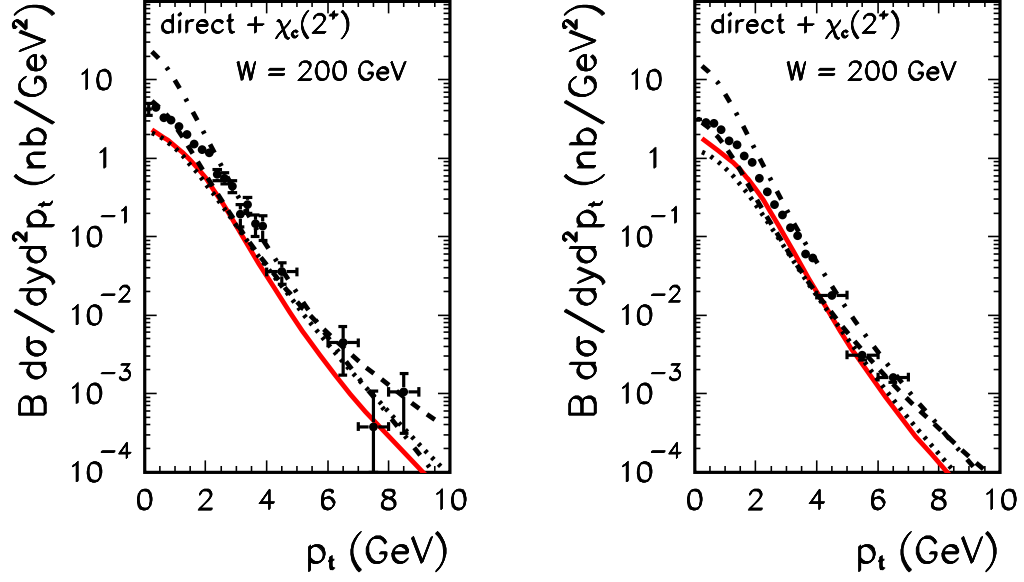


FIG. 10: Direct and  $\chi_c$ -decay contributions to transverse momentum distribution of  $J/\psi$  for different models of UGDFs for different intervals in rapidity: (a)  $-0.35 < y < 0.35$  (left panel), (b)  $1.2 < |y| < 2.2$  (right panel). The meaning of the curves is the same as in Fig. 5. The new PHENIX data are shown as full circles.

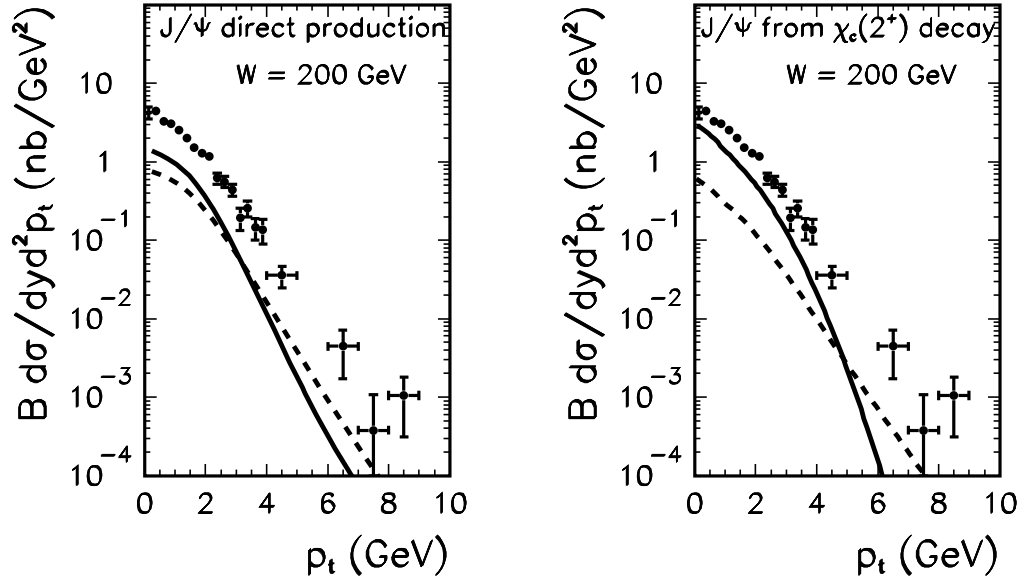


FIG. 11: Factorization scale dependence of the transverse momentum distribution for Kwieciński UGDF. The mid rapidity range  $-0.35 < y < 0.35$  was taken as an example. The left panel is for direct production and the right panel for the  $\chi_c(2^+)$  decay mechanism. The solid and dashed curves are for  $\mu^2 = 10 \text{ GeV}^2$  and for  $\mu^2 = 100 \text{ GeV}^2$ , respectively. In this calculation  $b_0 = 1 \text{ GeV}^{-1}$ .

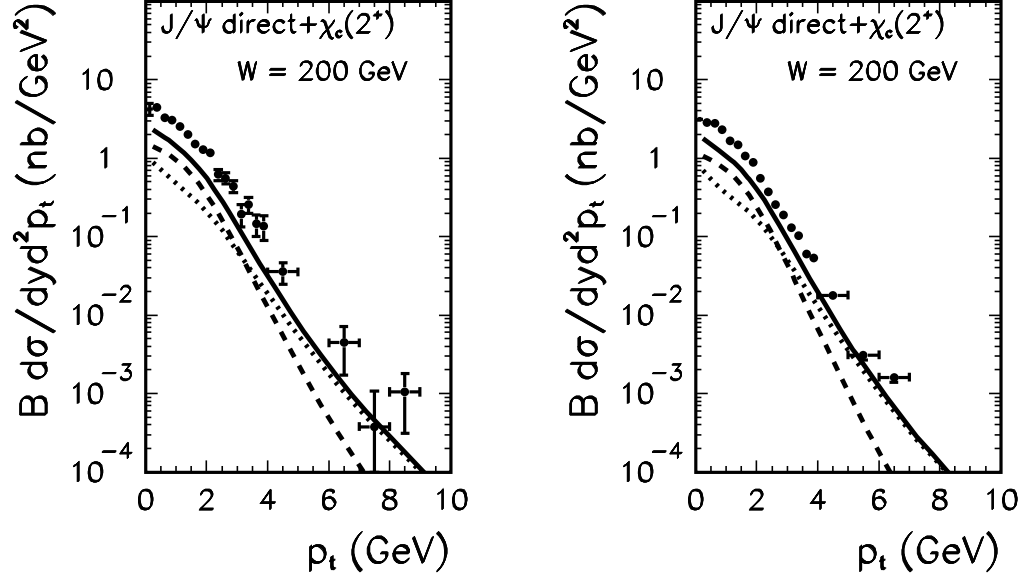


FIG. 12: Invariant cross section for the Kwieciński UGDF with running scale. The left panel is for central rapidity range ( $-0.35 < y < 0.35$ ) and the right panel for intermediate rapidity range ( $1.2 < y < 2.2$ ). The direct contribution is denoted by the dashed line, the  $\chi_c(2^+)$ -decay contribution by the dotted line and the sum of both by the solid line.

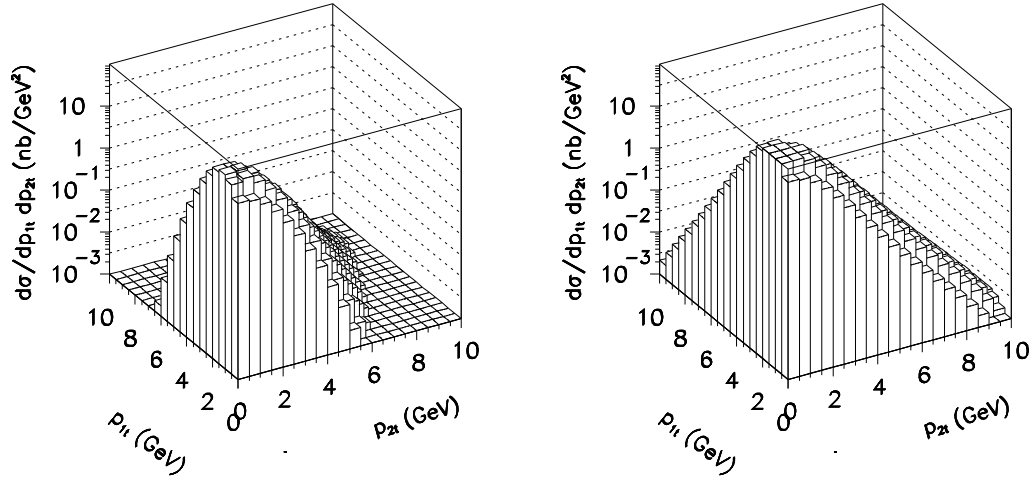


FIG. 13: Factorization scale dependence of the  $p_{J/\psi,t} \times p_{g,t}$  distribution for the Kwieciński UGDF. The left panel is for  $\mu^2 = 10 \text{ GeV}^2$  and the right panel is for  $\mu^2 = 100 \text{ GeV}^2$ .

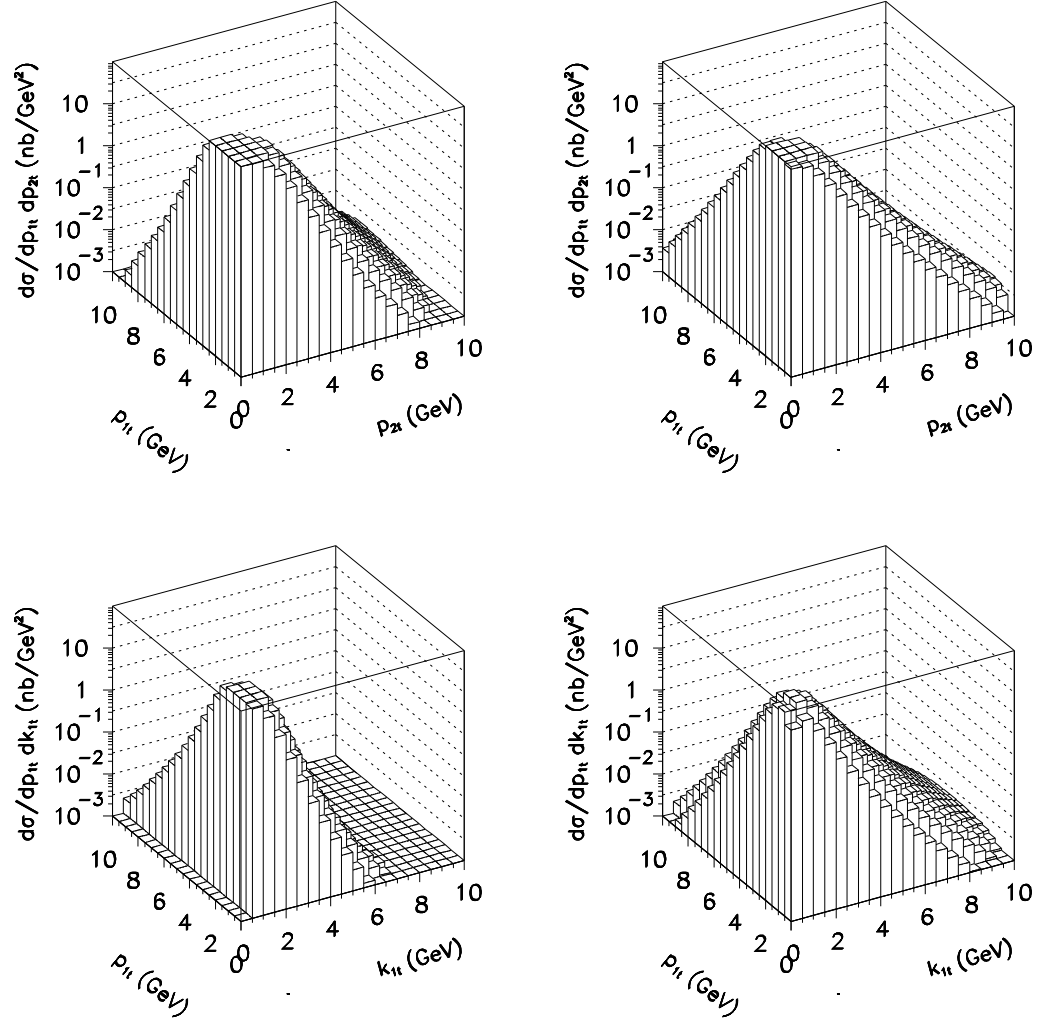


FIG. 14: Two-dimensional distribution of the  $J/\psi$  and gluon transverse momenta. The *left-top* panel is for Kwieciński UGDF (running scale) and matrix element gluon, the *right-top* panel is for the BFKL UGDF and matrix element gluon, the *left-bottom* panel is for the Kwieciński UGDF (running scale) and "last from the ladder" gluon and the *right-bottom* panel is for the BFKL UGDF and "last from the ladder" gluon.

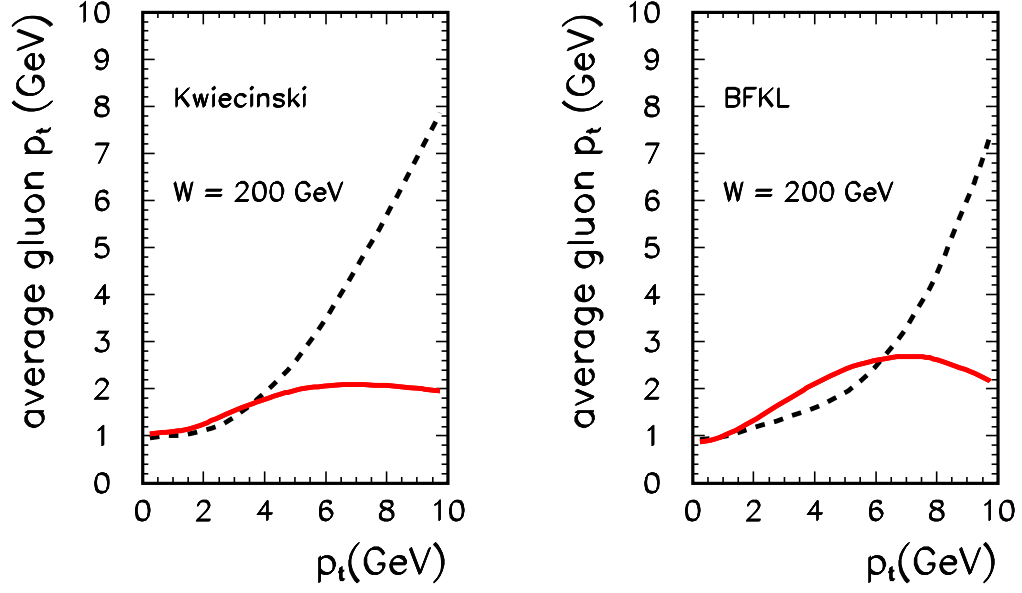


FIG. 15: Average transverse momenta of the ME (dashed) and LFL (solid) gluons as a function of the  $J/\psi$  transverse momentum for the Kwieciński UGDF with running scale (left panel) and the BFKL UGDF (right panel) at the RHIC energy  $W = 200$  GeV.

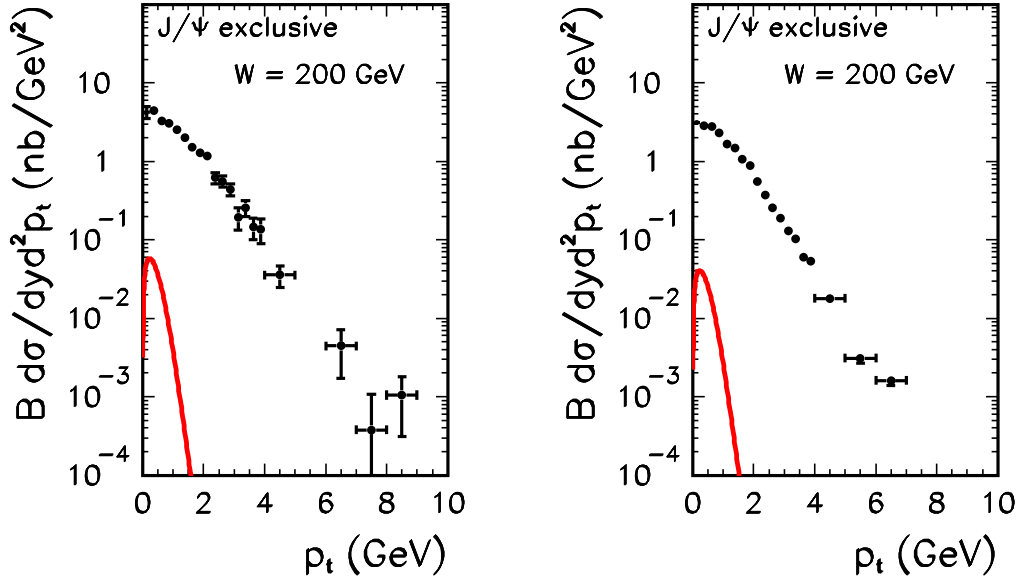


FIG. 16: Invariant cross section for the exclusive photoproduction mechanism. The left panel is for central rapidity range  $(-0.35 < y < 0.35)$  and the right panel for intermediate rapidity range  $(1.2 < y < 2.2)$ .

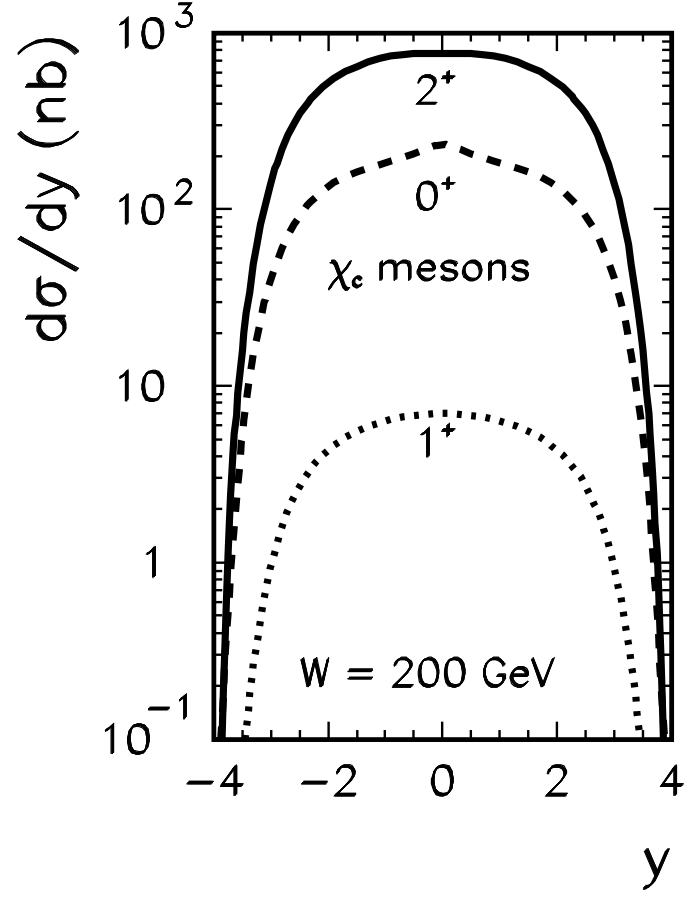


FIG. 17: Rapidity distribution of  $\chi_c(0^+)$  (dashed),  $\chi_c(1^+)$  (dotted) and  $\chi_c(2^+)$  (solid) for the RHIC energy obtained with the Kwieciński UGDF ( $b_0 = 1 \text{ GeV}^{-1}$ ,  $\mu^2 = p_t^2(\chi_c)$ ).

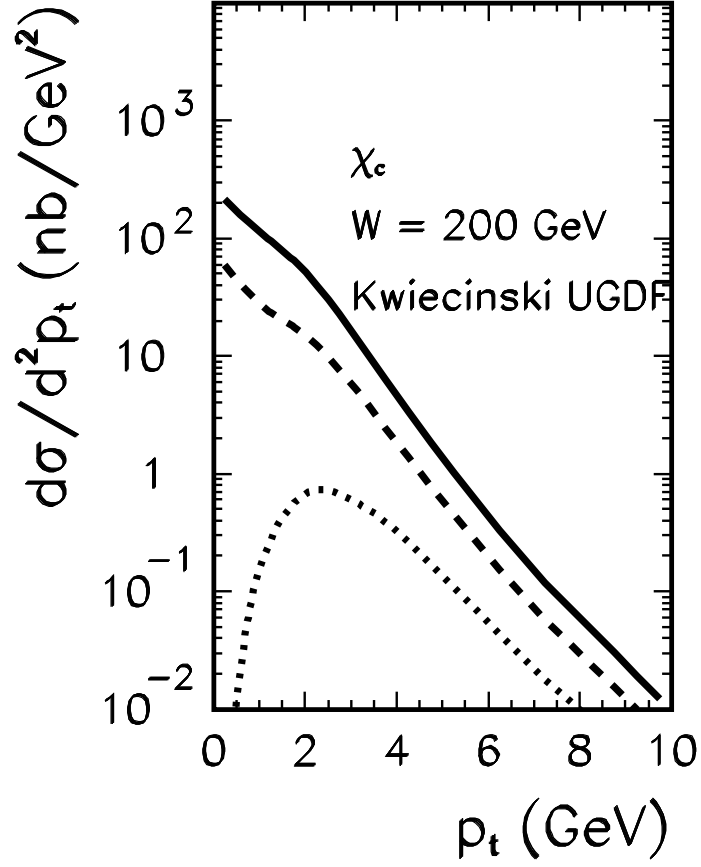


FIG. 18: Transverse momentum distribution of  $\chi_c(0^+)$  (dashed),  $\chi_c(1^+)$  (dotted) and  $\chi_c(2^+)$  (solid) for the RHIC energy obtained with the Kwieciński UGDF ( $b_0 = 1 \text{ GeV}^{-1}$ ,  $\mu^2 = p_t^2(\chi_c)$ ).

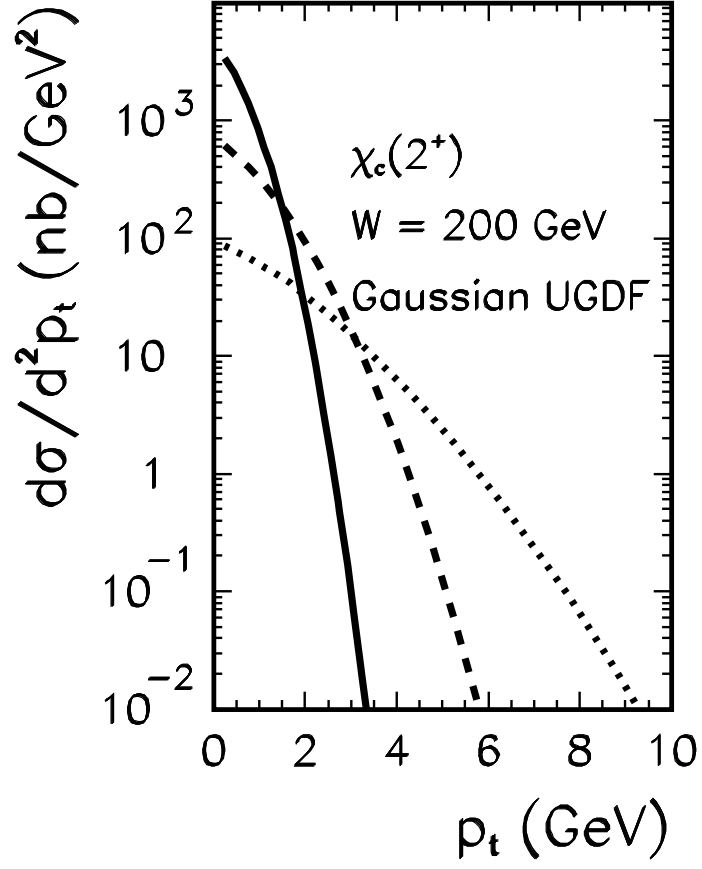


FIG. 19: Transverse momentum distribution of  $\chi_c(2^+)$  for the RHIC energy obtained with the Gaussian UGDF and different values of  $\sigma_0 = 0.5, 1.0, 2.0 \text{ GeV}$ .

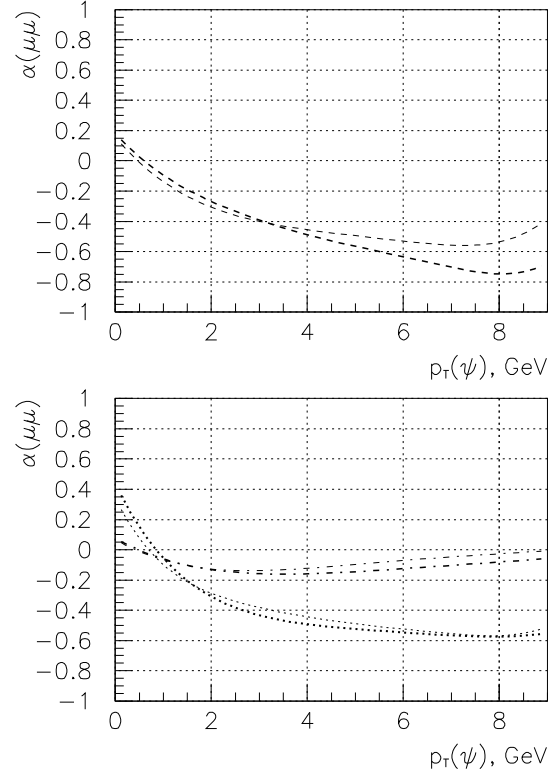


FIG. 20: Predictions for the spin-alignment parameter  $\alpha$  for  $J/\psi$  and  $W = 200$  GeV. Thick lines correspond to the JB parametrization [52] and the thin lines correspond to the derivative dGRV parametrization. The top panel is for direct contribution only. The bottom panel includes the feed-down from  $\chi_c$  decays taken into account. The dotted lines are for the quark spin conservation hypothesis, and the dash-dotted lines are for the full depolarization hypothesis.